

Exact polarizability and plasmon resonances of partly buried nanowires

Jesper Jung* and Thomas G. Pedersen

Department of Physics and Nanotechnology, Aalborg University, Skjernvej 4A, DK-9220 Aalborg Øst, Denmark and Interdisciplinary Nanoscience Center (iNANO), Denmark

*jung@nano.aau.dk

Abstract: The electrostatic polarizability for both vertical and horizontal polarization of two conjoined half-cylinders partly buried in a substrate is derived in an analytical closed-form expression. Using the derived analytical polarizabilities we analyze the localized surface plasmon resonances of three important metal nanowire configurations: (1) a half-cylinder, (2) a half-cylinder on a substrate, and (3) a cylinder partly buried in a substrate. Among other results we show that the substrate plays an important role for spectral location of the plasmon resonances. Our analytical results enable an easy, fast, and exact analysis of many complicated plasmonic nanowire configurations including nanowires on substrates. This is important both for comparison with experimental data, for applications, and as benchmarks for numerical methods.

© 2018 Optical Society of America

OCIS codes: (000.3860) Mathematical methods in physics; (240.6680) Surface plasmons; (230.5750) Resonators.

References and links

1. M. Faraday, "Experimental relations of gold (and other metals) to light," *Phil. Trans. R. Soc. Lond.* **147**, 145–181 (1857).
2. J. W. Strutt (Lord Rayleigh), "On the scattering of light by small particles," *Phil. Mag.* **41**, 447–454 (1871).
3. L. Lorenz, "Lysbevægelsen i og udenfor en af plane lysbølger belyst kugle," *K. Dan. Vidensk. Selsk. Skr.* **6**, 1–62 (1890).
4. G. Mie, "Beitrag zur Optik trüber Medien speziell kolloidaler Metallosungen," *Ann. Physik.* **330**, 337–445 (1908).
5. C. F. Bohren and D. R. Huffman, *Absorption and Scattering of Light by Small Particles* (Wiley, 1983).
6. L. Rayleigh, "The dispersal of light by a dielectric cylinder," *Phil. Mag.* **36**, 365–376 (1918).
7. J. R. Wait, "Scattering of a plane wave from a circular cylinder at oblique incidence," *Can. J. Phys.* **33**, 189–195 (1955).
8. H. C. van de Hulst, *Light Scattering by Small Particles* (Dover, 2000).
9. L. Novotny and B. Hecht, *Principles of Nano-Optics* (Cambridge University Press, 2006).
10. A. V. Zayats and I. I. Smolyaninov, "Near-field photonics: surface plasmon polaritons and localized surface plasmons," *J. Opt. A: Pure Appl. Opt.* **5**, S16-S50 (2003).
11. S. A. Maier and H. A. Atwater, "Plasmonics: Localization and guiding of electromagnetic energy in metal/dielectric structures," *J. Appl. Phys.* **98**, 011101 (2005).
12. W. A. Murray and W. L. Barnes, "Plasmonic materials," *Adv. Mater.* **19**, 3771–3782 (2007).
13. S. Lal, S. Link, and N. J. Halas, "Nano-optics from sensing to waveguiding," *Nat. Photon.* **1**, 641–648 (2007).
14. P. Muhschlegel, H.-J. Eisler, O. J. F. Martin, B. Hecht, and D. W. Pohl, "Resonant optical antennas," *Science* **308**, 1607–1609 (2005).
15. L. Novotny, "Effective wavelength scaling for optical antennas," *Phys. Rev. Lett.* **98**, 266802 (2007).
16. F. Hallermann, C. Rockstuhl, S. Fahr, G. Seifert, S. Wackerow, H. Graener G. V. Plessen, and F. Lederer, "On the use of localized plasmon polaritons in solar cells," *Phys. Stat. Sol. (a)* **12**, 2844–2861 (2008).
17. H. A. Atwater and A. Polman, "Plasmonics for improved photovoltaic devices," *Nat. Mater.* **9**, 205–213 (2010).

18. P. C. Waterman, "Surface fields and the T matrix," J. Opt. Soc. Am. A **16**, 2968–2977 (1999).
 19. A. V. Radchik, A. V. Paley, G. B. Smith, and A. V. Vagov, "Polarization and resonant absorption in intersecting cylinders and spheres," J. Appl. Phys. **76**, 4827–4835 (1994).
 20. A. Salandrino, A. Alu, and N. Engheta, "Parallel, series, and intermediate interconnects of optical nanocircuit elements. I. Analytical solution," J. Opt. Soc. Am. B **24**, 3007–3013 (2007).
 21. M Pitkonen, "A closed-form solution for the polarizability of a dielectric double half-cylinder," J. Electromagn. Waves Appl. **24**, 1267–1277 (2010).
 22. H. Kettunen, H. Wallen, and A. Sihvola, "Polarizability of a dielectric hemisphere," J. Appl. Phys. **102**, 044105 (2007).
 23. P. M. Morse and H. Feshbach, *Methods of Theoretical Physics, Part II* (McGraw-Hill Book Company Inc., 1953).
 24. H. E. Lockwood, *A Book of Curves* (Cambridge University Press, 1963).
 25. S. A. Maier, *Plasmonics: Fundamentals and Applications* (Springer, 2007).
 26. P. B. Johnson and R. W. Christy, "Optical constants of the noble metals," Phys. Rev. B **6**, 4370–4379 (1972).
-

1. Introduction

The optical properties of small structures have fascinated scientists for a long time. In 1857, Michael Faraday studied the interaction of light with colloidal metals [1] and in 1871 Lord Rayleigh presented an analytical analysis of light scattering from small spherical particles [2]. A full analytical analysis of spherical particles can be made using the Lorenz-Mie scattering theory [3–5]. Light scattering of a normal incidence plane wave by a small cylinder was addressed by Lord Rayleigh in 1918 [6] and extended to oblique incidence by J. R. Wait in 1955 [7]. Since then the problem of light scattering from small particles and cylinders has been revisited many times and is today well understood [5, 8, 9].

Due to the recent progress in the development of nanotechnologies, which has enabled fabrication of structures on the scale of a few nanometers, the interest in the optical properties of such structures is today enormous. In particular, metal nanostructures are intensively studied because they allow for resonant excitation of localized surface plasmons [10–13], i.e. collective excitations of the free conduction electrons that are resonantly coupled to the electromagnetic field. Both metal nanowires and -particles have several interesting applications as optical antennas [14, 15], within photovoltaics [16, 17], and many others (see e.g. Ref. [13] and references therein). Optimal design and fabrication of metal nanostructures for applications rely on accurate numerical simulations and theoretical predictions. Full numerical solution of the Maxwell equations for metal nanostructures is a demanding and time-consuming computational task. The huge field-gradients near e.g. metal corners require a very fine meshing in order to obtain reliable results. Thus, for these cases, accurate analytical models that predict the optical properties are very important, both for applications and as benchmarks for numerical methods.

In the present work, we analytically calculate the polarizability and the plasmon resonances of a geometry, which we name "the partly buried double half-cylinder". The geometry is illustrated schematically in Fig. 1. It consists of a double half-cylinder (a pair of conjoined half-cylinders) with optical properties described by the dielectric constants ϵ_1 and ϵ_2 , respectively. The double half-cylinder is placed in two semi-infinite half-spaces with optical properties given by the dielectric constants ϵ_3 and ϵ_4 . The simpler case of a half-cylinder [18] or a double half-cylinder in a *homogenous* surrounding has, to some extent, been analyzed before [19–21]. Also, a double half-sphere consisting of two joint hemispheres with different dielectric constants has been studied [22]. However, for this three dimensional problem no closed-form analytical solution was found [22]. In Ref. [20], two conjoined half-cylinders were analyzed using Kelvin inversion and Mellin transforms yielding a solution for the potential, however, only for a special resonant case where the two dielectric constants are of similar magnitude and opposite sign. Using the bipolar coordinate system [23, 24], cosine- and sine-transformations, a more general analysis of the double half-cylinder has recently been presented by Pitkonen [21]. To some extent, our analysis follows the lines of Pitkonen, in that we use bipolar coordinates, as

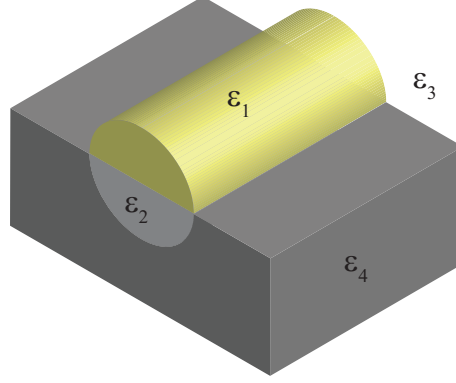


Fig. 1. Geometry of the partly buried double half-cylinder.

well as cosine- and sine-transformations. However, we consider a much more general geometry c.f. Fig. 1. Our approach e.g. enables analysis of a nanowire with the shape of a half-cylinder supported by a substrate. This is important because nanowires are often supported by a substrate and usually have cross-sectional shapes approximating half-circles. Compared to Pitkonen we also obtain much more compact expressions for the polarizabilities, i.e. we avoid using poly-logarithms as after reduction, only the natural logarithm is needed. Finally, we also analyze the plasmon resonances of the more general geometry in detail.

2. Theory

We start our analysis by assuming that the dielectric constants are linear, isotropic, homogeneous, and frequency dependent. To simplify the notation, the frequency dependence of dielectric constant $\varepsilon_i = \varepsilon_i(\omega)$ is implicitly assumed. We also assume that the cross section of the double half-cylinder is small compared to the wavelength, i.e. we take an electrostatic approach. In a static theory, $\nabla \times \mathbf{E}(\mathbf{r}) = 0$ and the electrostatic field can be expressed by means of the electrostatic potential $\mathbf{E}(\mathbf{r}) = -\nabla\phi(\mathbf{r})$. In each domain, the electrostatic potential must fulfill Laplace's equation $\nabla^2\phi(\mathbf{r}) = 0 \quad \forall \mathbf{r}$, with the boundary conditions $\phi_i = \phi_j$ and $\varepsilon_i\hat{n} \cdot \nabla\phi_i = \varepsilon_j\hat{n} \cdot \nabla\phi_j$ on S , where the subscripts i and j refer to the different domains (1,2,3, and 4) and S to the boundaries.

The first step of our analysis is to switch to bipolar coordinates u and v [23, 24], which are connected to rectangular coordinates via $x = \sinh u / (\cosh u - \cos v)$ and $y = \sin v / (\cosh u - \cos v)$. The domains of u and v for the different regions are shown in Fig. 2. First we consider the case where the incident field is polarized along the y axis. Such a field will induce a vertically oriented dipole moment in the double half-cylinder. Thus, we look for solutions that are even functions of x and, hence, u . For a unit amplitude incident field $\mathbf{E}_0 = \hat{y}$ the incident potential is given as

$$\phi_0(x, y) = -y \begin{cases} 1 & \text{for } y > 0 \\ \frac{\varepsilon_3}{\varepsilon_4} & \text{for } y < 0 \end{cases} ,$$

which transforms into

$$\phi_0(u, v) = -\frac{\sin v}{\cosh u - \cos v} \begin{cases} 1 & \text{for } v > 0 \\ \frac{\varepsilon_3}{\varepsilon_4} & \text{for } v < 0 \end{cases} .$$

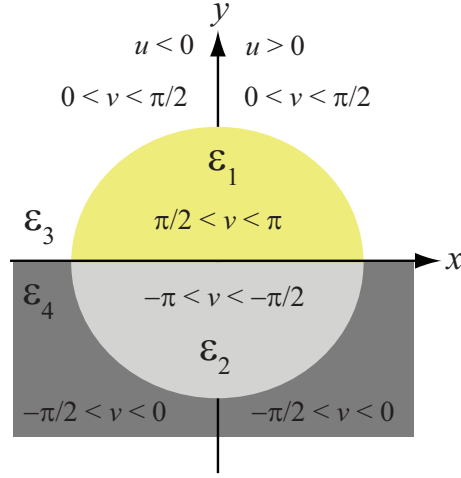


Fig. 2. Cross section of the partly buried double half-cylinder geometry. In bipolar coordinates (u and v), the four different regions in the xy plane are given as $\epsilon_1 : \{-\infty < u < \infty \text{ and } \pi/2 < v < \pi\}$, $\epsilon_2 : \{-\infty < u < \infty \text{ and } -\pi < v < -\pi/2\}$, $\epsilon_3 : \{-\infty < u < \infty \text{ and } 0 < v < \pi/2\}$, and $\epsilon_4 : \{-\infty < u < \infty \text{ and } -\pi/2 < v < 0\}$.

In each of the four regions, the scattered part of the potential is expanded as

$$\phi_i(u, v) = \int_0^\infty \bar{\phi}_i(\lambda, v) \cos(\lambda u) d\lambda,$$

with $\bar{\phi}_i(\lambda, v) = c_i(\lambda) \cosh(\lambda v) + s_i(\lambda) \sinh(\lambda v)$ and the inverse transformation given as

$$\bar{\phi}_i(\lambda, v) = \frac{2}{\pi} \int_0^\infty \phi_i(u, v) \cos(\lambda u) du.$$

The vertical polarizability α_v of the partly buried double half-cylinder can be found as (see Appendix)

$$\alpha_v = 4\pi \int_0^\infty \lambda s_3(\lambda) d\lambda. \quad (1)$$

Note that the polarizability in Eq. (1) is the normalized polarizability. To convert into standard units α_v should be multiplied by the radius of the cylinder squared. By solving the equation system formed from the boundary conditions of the potential and its normal derivative (see Appendix for details), $s_3(\lambda)$ can be calculated, and by performing the integral in Eq. (1) we find the vertical polarizability as

$$\alpha_v = \frac{2\pi}{\epsilon_1 \epsilon_2 (\epsilon_3 + \epsilon_4) + (\epsilon_1 + \epsilon_2) \epsilon_3 \epsilon_4} \times \left[\epsilon_1 \epsilon_2 (\epsilon_3 + \epsilon_4) - (\epsilon_1 + \epsilon_2) \epsilon_3 \epsilon_4 - \frac{2(\epsilon_1 + \epsilon_2) \epsilon_3 \epsilon_4}{\pi^2} \ln^2 \left(\frac{A+B}{A-B+2i\sqrt{AB}} \right) \right], \quad (2)$$

where $A = (\epsilon_1 + \epsilon_2 + \epsilon_3 + \epsilon_4)[\epsilon_1 \epsilon_2 (\epsilon_3 + \epsilon_4) + (\epsilon_1 + \epsilon_2) \epsilon_3 \epsilon_4]$ and $B = (\epsilon_1 \epsilon_4 - \epsilon_2 \epsilon_3)^2$. It should be noted that the result presented by Pitkonen in Ref. [21] for the simpler case of $\epsilon_3 = \epsilon_4$ is consistent with Eq. (2). This can be demonstrated using identities for polylogarithms to rewrite

Pitkonen's result in terms of the natural logarithm. From Eq. (2) the resonance condition can be identified as

$$\varepsilon_1 \varepsilon_2 (\varepsilon_3 + \varepsilon_4) + (\varepsilon_1 + \varepsilon_2) \varepsilon_3 \varepsilon_4 = 0. \quad (3)$$

For ordinary dielectric surroundings $\varepsilon_3, \varepsilon_4 > 0$, the resonance condition can only be fulfilled if the dielectric constant of the partly buried double half-cylinder is negative e.g. if the cylinder is made of a free electron-like metal as silver or gold. In this case, the resonances are dipole surface plasmon modes that arise due to the interaction of the free conduction electrons in the metal cylinder with the time-dependent incident field. The plasmon resonance conditions for a vertically polarized incident field for some special geometries are presented in Table 1. Note

Table 1. Plasmon resonance conditions for vertically induced dipole moments.

Description	Dielectric constants	Resonance condition
cylinder	$\varepsilon_1 = \varepsilon_2 = \varepsilon$ and $\varepsilon_3 = \varepsilon_4 = \varepsilon_h$	$\varepsilon = -\varepsilon_h$
partly buried cylinder	$\varepsilon_1 = \varepsilon_2 = \varepsilon$ and $\varepsilon_4 = \varepsilon_h$	$\varepsilon = -2\varepsilon_3 \varepsilon_h / (\varepsilon_3 + \varepsilon_h)$
half-cylinder	$\varepsilon_1 = \varepsilon$ and $\varepsilon_2 = \varepsilon_3 = \varepsilon_4 = \varepsilon_h$	$\varepsilon = -\varepsilon_h / 3$
half-cylinder on substrate	$\varepsilon_1 = \varepsilon$ and $\varepsilon_2 = \varepsilon_4 = \varepsilon_h$	$\varepsilon = -\varepsilon_h \varepsilon_3 / (2\varepsilon_3 + \varepsilon_h)$

that the well known result $\varepsilon = -\varepsilon_h$ for a homogenous cylinder [9] is obtained from our general result.

For a horizontally polarized incident field i.e. $\mathbf{E}_0(\mathbf{r}) = \hat{x}$ we have

$$\phi_0(u, v) = -\frac{\sinh u}{\cosh u - \cos v}.$$

Such a field will induce a horizontally oriented dipole moment in the cylinder and we therefore look for solutions that are odd functions of x and, hence, u . In each of the four regions, we expand the scattered potential as

$$\phi_i(u, v) = \int_0^\infty \bar{\phi}_i(\lambda, v) \sin(\lambda u) d\lambda.$$

Similarly to the vertically polarized case, the horizontal polarizability may be found as (see Appendix for details)

$$\alpha_h = 4\pi \int_0^\infty \lambda c_3(\lambda) d\lambda. \quad (4)$$

From the equations formed from the boundary conditions of the potential and its normal derivative, $c_3(\lambda)$ can be calculated (see Appendix). By performing the integral in Eq. (4), we find the horizontal polarizability as

$$\alpha_h = \frac{2\pi}{\varepsilon_1 + \varepsilon_2 + \varepsilon_3 + \varepsilon_4} \left[\varepsilon_1 + \varepsilon_2 - \varepsilon_3 - \varepsilon_4 + \frac{2(\varepsilon_1 + \varepsilon_2)}{\pi^2} \ln^2 \left(\frac{A+B}{A-B+2i\sqrt{AB}} \right) \right]. \quad (5)$$

It should be noted that there exists a simple symmetry between α_h and α_v . By replacing ε_i with $1/\varepsilon_i$ and changing the sign, α_v transforms into α_h and vice versa. For a horizontally polarized induced dipole moment the plasmon resonance condition simply states that the sum of all the dielectric constants must be zero

$$\varepsilon_1 + \varepsilon_2 + \varepsilon_3 + \varepsilon_4 = 0. \quad (6)$$

Special cases for simpler geometries are given in Table 2. Equations (2), (3), (5), and (6) represent the principal results of this work.

Table 2. Plasmon resonance conditions for horizontally induced dipole moments.

Description	Dielectric constants	Resonance condition
cylinder	$\epsilon_1 = \epsilon_2 = \epsilon$ and $\epsilon_3 = \epsilon_4 = \epsilon_h$	$\epsilon = -\epsilon_h$
partly buried cylinder	$\epsilon_1 = \epsilon_2 = \epsilon$ and $\epsilon_4 = \epsilon_h$	$\epsilon = -(\epsilon_3 + \epsilon_h)/2$
half-cylinder	$\epsilon_1 = \epsilon$ and $\epsilon_2 = \epsilon_3 = \epsilon_4 = \epsilon_h$	$\epsilon = -3\epsilon_h$
half-cylinder on substrate	$\epsilon_1 = \epsilon$ and $\epsilon_2 = \epsilon_4 = \epsilon_h$	$\epsilon = -(2\epsilon_h + \epsilon_3)$

3. Results

In Figs. 3, 4, and 5, we illustrate the polarizability for three important geometries. In order to easily identify the plasmon resonances, we first calculate the polarizability as a function of the real part ϵ_r of the dielectric constant of the cylinder (or half-cylinder) with a fixed small imaginary part as $\epsilon = \epsilon_r + 0.01i$. As we are interested in the plasmon response of the system we consider negative ϵ_r . First we consider the geometry of a half-cylinder in a homogenous surrounding with $\epsilon_h = 1$ (Fig. 3). The result shows that both the real and the imaginary part

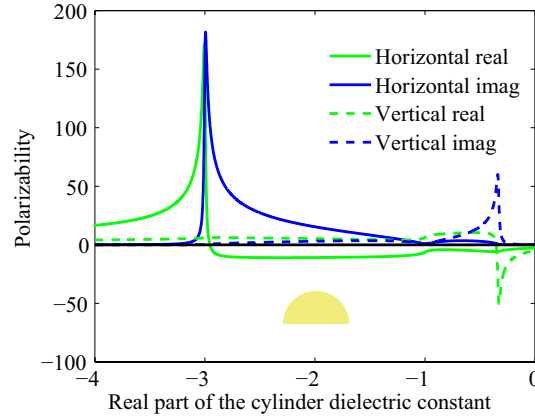


Fig. 3. Polarizability as a function of ϵ_r of a half-cylinder with $\epsilon_1 = \epsilon_r + 0.01i$ in a surrounding medium described by $\epsilon_2 = \epsilon_3 = \epsilon_4 = 1$.

of the vertical polarizability display a resonant behavior at $\epsilon_r = -\epsilon_h/3 = -1/3$. Such a resonance is commonly referred to as a dipole surface plasmon resonance [25]. Notice how the imaginary part of the polarizability is always positive as it should be for ordinary lossy materials. This is contrary to the numerical results presented by Pitkonen [21], which display strange negative imaginary parts of the polarizability. Note also how the real part of the polarizability changes sign across the plasmon resonance. For horizontally induced dipole moments the surface plasmon resonance of the metallic half-cylinder is located at $\epsilon_r = -3\epsilon_h = -3$. This plasmon resonance is clearly visible in both real and imaginary parts of the polarizability.

The second geometry that we consider is a half-cylinder supported by a substrate (Fig. 4). Such a configuration is of particular interest in relation to experimental work. Firstly, because nanowires are usually supported by substrates and, secondly, because nanowires often have cross sectional shapes similar to half-circles. Here, we consider the case of an air ($\epsilon_3 = 1$) superstrate and quartz ($\epsilon_2 = \epsilon_4 = \epsilon_h = 1.5^2$) substrate. For vertical polarization the configuration has a surface plasmon resonance at $\epsilon_r = -\epsilon_h\epsilon_3/(2\epsilon_3 + \epsilon_h) \approx -0.53$. This resonance is clearly seen in both real and imaginary parts of the polarizability. For the horizontal case the surface

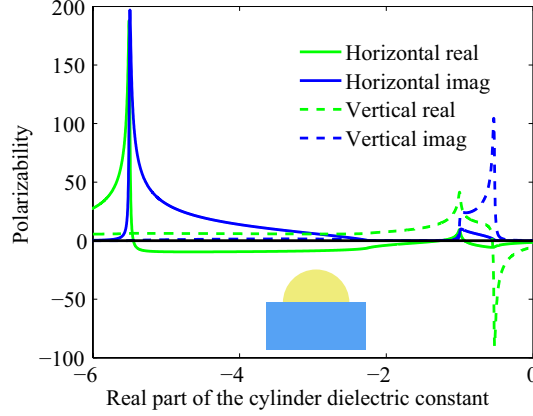


Fig. 4. Polarizability as a function of ϵ_r of a half-cylinder laying on a substrate. The dielectric constants of the half-cylinder, the substrate, and the superstrate are $\epsilon_1 = \epsilon_r + 0.01i$, $\epsilon_2 = \epsilon_4 = 1.5^2$, and $\epsilon_3 = 1$, respectively.

plasmon resonance is located at $\epsilon = -(2\epsilon_h + \epsilon_3) = -5.5$. Note that when compared to the half-cylinder in air (Fig. 3), the plasmon resonances shift significantly, in particular, for the case of a horizontally polarized driving field. This is an important finding because it underlines the fact that the substrate plays a crucial role when the spectral location of the plasmon resonances of metallic nanostructures are established.

The third geometry that we consider is a full cylinder ($\epsilon_1 = \epsilon_2 = \epsilon$) partly buried in a quartz substrate ($\epsilon_4 = 1.5^2$ and $\epsilon_3 = 1$). The polarizability is presented in Fig. 5. For the case of verti-

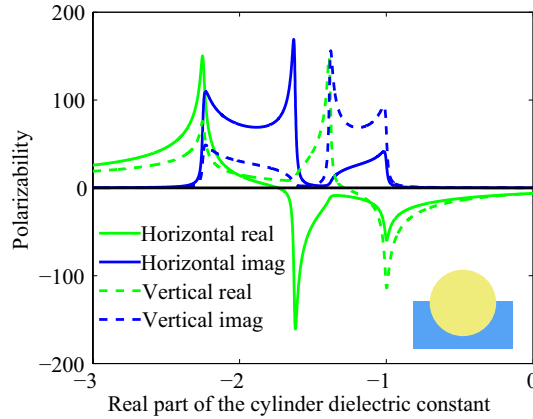


Fig. 5. Polarizability as a function of ϵ_r of a partly buried cylinder with $\epsilon_1 = \epsilon_2 = \epsilon_r + 0.01i$. The dielectric constants of the sub- and superstrate are $\epsilon_4 = 1.5^2$ and $\epsilon_3 = 1$, respectively.

cal polarization this configuration has a dipole plasmon resonance at $\epsilon = -2\epsilon_3\epsilon_4/(\epsilon_3 + \epsilon_4) \approx -1.38$. For horizontal polarization the plasmon resonance is located at $\epsilon = -(\epsilon_3 + \epsilon_4)/2 = -1.625$. For this geometry the polarizability is more complicated. Three peaks in both the real and the imaginary part of the polarizability can be identified from the figure, resulting in a large polarizability over a wide range of ϵ_r .

Next, we have calculated the polarizability as a function of wavelength for the same three geometries in the case of silver in air or on quartz. The data for the dielectric constant of silver is taken from the experiments of Johnson and Christy [26]. For the half-cylinder the result is presented in Fig. 6 (a). The horizontal polarizability displays a clear resonance around 370 nm.

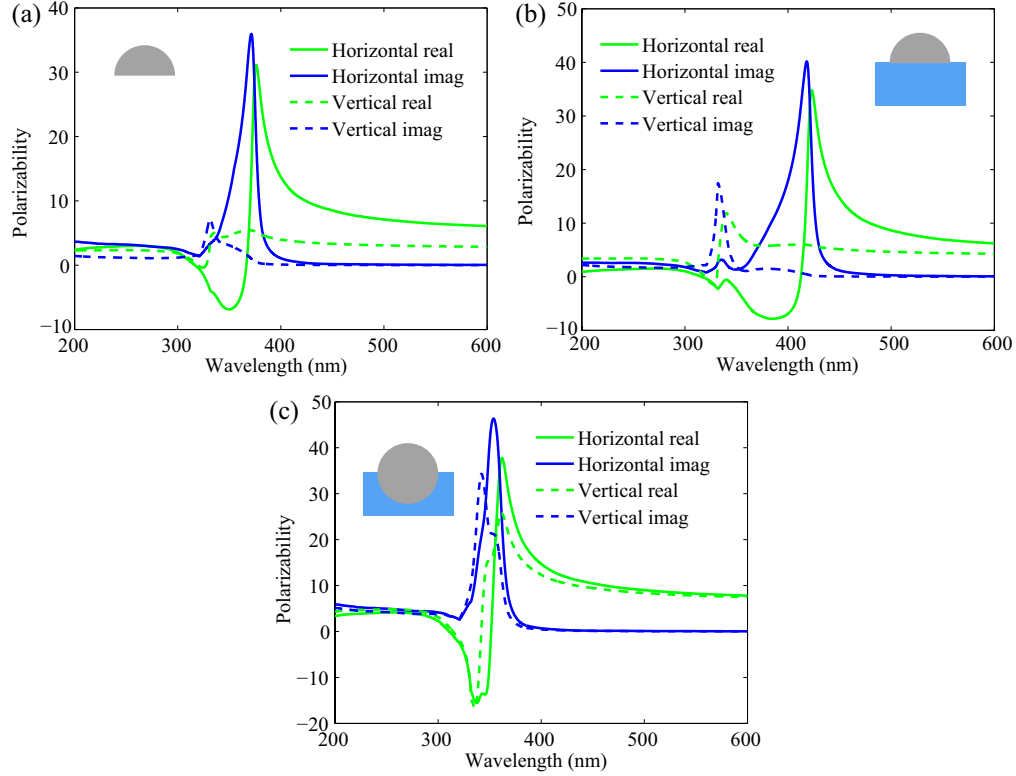


Fig. 6. Polarizability as a function of wavelength for (a) a silver half-cylinder, (b) a silver half-cylinder on a quartz substrate, and (c) a silver cylinder partly buried in a quartz substrate.

This corresponds nicely to the wavelength where the real part of the dielectric constant of silver equals -3 . The vertical response shows a resonance at approximately 330 nm, which is where the real part of the dielectric constant of silver is $-1/3$. For a half-cylinder supported by a quartz ($\epsilon_h = 1.5^2$) substrate the polarizability is presented in Fig. 6 (b). Note how the resonance in the horizontal polarizability has red-shifted approximately 50 nm due to the presence of the quartz substrate. The resonance wavelength is now close to 420 nm, which is where the real part of the dielectric constant of silver is approximately -5.5 . When compared to the half-cylinder in homogenous space, the vertical resonance of the half-cylinder on quartz does not red-shift significantly. The explanation for the larger red-shift seen in the horizontal polarizability is that a larger part of the field is within the substrate for a horizontal dipole moment than for a vertical one. For the partly buried cylinder the polarizabilities as a function of wavelength are presented in Fig. 6 (c). The result shows that the resonances in the vertical and the horizontal polarizabilities are similar to each other. This might be expected because for both polarizations approximately half of the plasmon field will be within the substrate.

4. Conclusion

In conclusion, we have presented an analytical study of the electrostatic polarizability of a general geometry consisting of two conjoined half-cylinders embedded in a reference structure of two semi-infinite half-spaces. The analysis is performed using bipolar coordinates, cosine-, and sine-transformations and closed-form expressions for the polarizabilities are presented for both polarizations using elementary functions. For cylinders (or half-cylinders) with negative dielectric constant the resonance criterion for the surface plasmon resonance is examined and several special cases of the general geometry are considered. The present results provide analytical predictions of plasmon resonances of several important structures within nanowire plasmonics.

5. Appendix

5.1. Vertical polarization

The vertical polarizability α_v of the partly buried double half-cylinder is obtained by comparing the far-field expression of the scattered potential on the y axis with the scattered potential from a line dipole $\phi(\mathbf{r}) = \mathbf{p}_v \cdot \hat{r}/(2\pi r)$, where $\mathbf{p}_v = \alpha_v \cdot \mathbf{E}_0$ is the induced dipole moment with the constant incident electric field $\mathbf{E}_0 = -\nabla\phi_0(\mathbf{r})$. On the y axis $x = 0$ and, hence, $u = 0$, thus we find $y = \sin v/(1 - \cos v)$, which in the far field should be large $y \gg 1$. This means that $v \ll 1$. In this limit, we Taylor expand the sine and cosine functions to find $v \approx 2/y$. Using $\sinh(v\lambda) \approx v\lambda$ and $\cosh(v\lambda) \approx 1$ we find the scattered far-field potential on the y axis as

$$\phi_3^{\text{ff}} = \frac{2}{y} \int_0^\infty \lambda s_3(\lambda) d\lambda + \int_0^\infty c_3(\lambda) d\lambda,$$

where the last integral just is a constant contribution to the potential. This constant is without physical significance as $\mathbf{E}(\mathbf{r}) = -\nabla\phi(\mathbf{r})$. By comparing with the potential of a vertically oriented line dipole $\phi(0, y) = p_v/(2\pi y)$ the vertical polarizability is easily found as

$$\alpha_v = 4\pi \int_0^\infty \lambda s_3(\lambda) d\lambda.$$

Similarly, $s_3(\lambda)$ can be calculated from the equation sets formed from the boundary conditions for the potential and its normal derivative. By introducing the constants $\gamma = \cosh(\lambda\pi/2)$ and $\xi = \sinh(\lambda\pi/2)$ we find from the continuity of the potential across the boundaries

$$\begin{aligned} c_1(\lambda)\gamma + s_1(\lambda)\xi &= c_3(\lambda)\gamma + s_3(\lambda)\xi, \\ c_2(\lambda)\gamma - s_2(\lambda)\xi &= c_4(\lambda)\gamma - s_4(\lambda)\xi, \\ c_1(\lambda)(\gamma^2 + \xi^2) + s_1(\lambda)2\gamma\xi &= c_2(\lambda)(\gamma^2 + \xi^2) - s_2(\lambda)2\gamma\xi, \\ c_3(\lambda) &= c_4(\lambda), \end{aligned} \tag{7}$$

where we have used that $\cosh(\lambda\pi) = \gamma^2 + \xi^2$ and $\sinh(\lambda\pi) = 2\xi\gamma$. From the transformed incident potential we find

$$\frac{\partial\phi_0(u, v)}{\partial v} = \left[-\frac{\cos v}{\cosh u - \cos v} + \frac{\sin^2 v}{(\cosh u - \cos v)^2} \right] \cdot \begin{cases} 1 & \text{for } v > 0 \\ \frac{\epsilon_3}{\epsilon_4} & \text{for } v < 0 \end{cases}.$$

We need four expressions

$$\begin{aligned} \frac{\partial}{\partial v} \phi_0\left(u, \frac{\pi}{2}\right) &= \frac{1}{\cosh^2 u}, & \frac{\partial}{\partial v} \phi_0\left(u, -\frac{\pi}{2}\right) &= \frac{\epsilon_3}{\epsilon_4 \cosh^2 u}, \\ \frac{\partial}{\partial v} \phi_0(u, \pi) &= \frac{1}{1 + \cosh u}, & \text{and } \frac{\partial}{\partial v} \phi_0(u, -\pi) &= \frac{\epsilon_3}{\epsilon_4(1 + \cosh u)} \end{aligned}$$

that transform into

$$\begin{aligned}\frac{\partial}{\partial v}\bar{\phi}_0\left(\lambda, \frac{\pi}{2}\right) &= \frac{\lambda}{\xi}, \quad \frac{\partial}{\partial v}\bar{\phi}_0\left(\lambda, -\frac{\pi}{2}\right) = \frac{\varepsilon_3\lambda}{\varepsilon_4\xi}, \\ \frac{\partial}{\partial v}\bar{\phi}_0(\lambda, \pi) &= \frac{\lambda}{\gamma\xi}, \quad \text{and} \quad \frac{\partial}{\partial v}\bar{\phi}_0(\lambda, -\pi) = \frac{\varepsilon_3\lambda}{\varepsilon_4\gamma\xi}.\end{aligned}$$

We also need

$$\frac{\partial\bar{\phi}_i(\lambda, v)}{\partial v} = \lambda [c_i(\lambda) \sinh(\lambda v) + s_i(\lambda) \cosh(\lambda v)].$$

Given these equations it is straightforward to use the boundary conditions for the normal derivative of the potential to set up

$$\begin{aligned}\varepsilon_1 \left[c_1(\lambda)\xi + s_1(\lambda)\gamma + \frac{1}{\xi} \right] &= \varepsilon_3 \left[c_3(\lambda)\xi + s_3(\lambda)\gamma + \frac{1}{\xi} \right], \\ \varepsilon_2 \left[-c_2(\lambda)\xi + s_2(\lambda)\gamma + \frac{\varepsilon_3}{\varepsilon_4\xi} \right] &= \varepsilon_4 \left[-c_4(\lambda)\xi + s_4(\lambda)\gamma + \frac{\varepsilon_3}{\varepsilon_4\xi} \right], \\ \varepsilon_1 \left[c_1(\lambda)2\xi\gamma + s_1(\lambda)(\gamma^2 + \xi^2) + \frac{1}{\xi\gamma} \right] &= \varepsilon_2 \left[-c_2(\lambda)2\xi\gamma + s_2(\lambda)(\gamma^2 + \xi^2) + \frac{\varepsilon_3}{\varepsilon_4\xi\gamma} \right], \\ \varepsilon_3 s_3(\lambda) &= \varepsilon_4 s_4(\lambda).\end{aligned}\tag{8}$$

From the equation set formed by Eqs. (7) and (8), $s_3(\lambda)$ can be found as

$$s_3(\lambda) = \frac{1}{\gamma\xi} \frac{-(\varepsilon_1\varepsilon_4 - \varepsilon_2\varepsilon_3)^2 + (\varepsilon_1 + \varepsilon_2)[\varepsilon_1\varepsilon_2(\varepsilon_3 + \varepsilon_4) - \varepsilon_3\varepsilon_4(\varepsilon_1 + \varepsilon_2 + \varepsilon_3 + \varepsilon_4) + \varepsilon_2\varepsilon_3^2 + \varepsilon_1\varepsilon_4^2]\gamma^2}{(\varepsilon_1\varepsilon_4 - \varepsilon_2\varepsilon_3)^2\xi^2 + (\varepsilon_1 + \varepsilon_2 + \varepsilon_3 + \varepsilon_4)[\varepsilon_1\varepsilon_2(\varepsilon_3 + \varepsilon_4) + (\varepsilon_1 + \varepsilon_2)\varepsilon_3\varepsilon_4]\gamma^2}.$$

5.2. Horizontal polarization

The horizontal polarizability is found by comparing the far-field expression of the scattered potential close to the y axis ($x \approx 0$) with the scattered potential of a horizontal line dipole, which for x small is given as $\phi(x \approx 0, y) = xp_h/(2\pi y^2)$. In the far field, where $y \gg 1$, we again find $v = 2/y \ll 1$ and for $x \approx 0$ we also have $u \approx 0$. With these limits, by using the connection between bipolar and rectangular coordinates and Taylor expanding the sine and cosine functions, we find $x/y \approx u/v$, which yields $u \approx 2x/y^2$. Now by approximating $\cosh(v\lambda) \approx 1$ we find the far-field expression of the scattered potential close to the y axis as

$$\phi_3^{\text{ff}} = \frac{2x}{y^2} \int_0^\infty \lambda c_3(\lambda) d\lambda,$$

and thus the horizontal polarizability

$$\alpha_h = 4\pi \int_0^\infty \lambda c_3(\lambda) d\lambda.$$

For horizontal polarization we choose the incident field as $\mathbf{E}_0(\mathbf{r}) = \hat{x}$, which yields

$$\frac{\partial}{\partial v}\phi_0(u, v) = \frac{\sinh u \sin v}{(\cosh u - \cos v)^2}.$$

Thus, we find

$$\frac{\partial}{\partial v}\phi_0(u, \pi) = \frac{\partial}{\partial v}\phi_0(u, -\pi) = \frac{\partial}{\partial v}\phi_0(u, 0) = 0,$$

and

$$\frac{\partial}{\partial v} \phi_0 \left(u, \pm \frac{\pi}{2} \right) = \pm \frac{\sinh u}{\cosh^2 u} \Rightarrow \frac{\partial}{\partial v} \bar{\phi}_0 \left(\lambda, \pm \frac{\pi}{2} \right) = \pm \frac{\lambda}{\gamma}.$$

The continuity equations for the potential are the same as for the vertical case, Eq. (7), but the boundary conditions for the normal derivative now lead to

$$\begin{aligned} \varepsilon_1 \left[c_1(\lambda) \xi + s_1(\lambda) \gamma + \frac{1}{\gamma} \right] &= \varepsilon_3 \left[c_3(\lambda) \xi + s_3(\lambda) \gamma + \frac{1}{\gamma} \right], \\ \varepsilon_2 \left[-c_2(\lambda) \xi + s_2(\lambda) \gamma - \frac{1}{\gamma} \right] &= \varepsilon_4 \left[-c_4(\lambda) \xi + s_4(\lambda) \gamma - \frac{1}{\gamma} \right], \\ \varepsilon_1 \left[c_1(\lambda) 2\xi \gamma + s_1(\lambda) (\gamma^2 + \xi^2) \right] &= \varepsilon_2 \left[-c_2(\lambda) 2\xi \gamma + s_2(\lambda) (\gamma^2 + \xi^2) \right], \\ \varepsilon_3 s_3(\lambda) &= \varepsilon_4 s_4(\lambda). \end{aligned} \quad (9)$$

From the equation set formed by Eqs. (7) and (9) we find $c_3(\lambda)$ as

$$c_3(\lambda) = \frac{1}{\gamma \xi} \frac{-(\varepsilon_1 \varepsilon_4 - \varepsilon_2 \varepsilon_3)^2 \xi^2 + (\varepsilon_1 + \varepsilon_2 - \varepsilon_3 - \varepsilon_4) [\varepsilon_1 \varepsilon_2 (\varepsilon_3 + \varepsilon_4) + (\varepsilon_1 + \varepsilon_2) \varepsilon_3 \varepsilon_4] \gamma^2}{(\varepsilon_1 \varepsilon_4 - \varepsilon_2 \varepsilon_3)^2 \xi^2 + (\varepsilon_1 + \varepsilon_2 + \varepsilon_3 + \varepsilon_4) [\varepsilon_1 \varepsilon_2 (\varepsilon_3 + \varepsilon_4) + (\varepsilon_1 + \varepsilon_2) \varepsilon_3 \varepsilon_4] \gamma^2}.$$

Again, note the simple symmetry between $c_3(\lambda)$ and $s_3(\lambda)$. By changing the sign and substituting ε_i with $1/\varepsilon_i$, $c_3(\lambda)$ transforms into $s_3(\lambda)$ and vice versa.

6. Acknowledgments

The authors gratefully acknowledge support from the project ‘‘Localized-surface plasmons and silicon thin-film solar cells - PLATOS’’ financed by the Villum foundation.